Catal Lett (2009) 128:40–48
DOI 10.1007/s10562-008-9712-1

Reforming of Model Gasification Tar Compounds

Agata Łamacz · Andrzej Krztoń · Andrea Musi · Patrick Da Costa

Received: 14 July 2008 / Accepted: 26 September 2008 / Published online: 7 November 2008

Abstract Gasification tar, causing various process equipment problems, is an undesirable product during biomass gasification therefore catalysts for its decomposition are needed. Toluene as a model tar compound was tested on steam reforming reaction using ceria-zirconia based Ni and Co catalysts.

Keywords Biomass · Toluene steam reforming · $Ni/CeZrO_2$ · $Co/CeZrO_2$

1 Introduction

Beside of hydropower, solar, and wind, biomass is found to be a very good source of renewable energy. Its main advantage over fossil fuels is neutral emission of greenhouse gas such as CO_2. Due to increasing petroleum price, biomass process is getting more and more eligible [1, 2]. Biomass gasification has attracted a lot of interest by producing a gas rich in CO and H_2 which is used for chemicals production, Fischer-Tropsch and methanol synthesis [3]. Among CO and H_2, gasification products are CO_2, water, nitrogen (in case of air application), small amount of methane, and higher hydrocarbons. The impurities present in the gas consist of ash, volatile alkali metals, and tar, which is a complex mixture of aromatics [1]. Depending on the type of gasifier and feedstock characteristics, concentrations of gas impurities range from 5 to 30 g/N m^3 for particles [4] and from 0.5 to 30 g/N m^3 for volatile alkali metals [5]. In fluid bed gasifiers tar content varies from 5 to 75 g/N m^3 [6, 7], what exceeds the maximum allowed for diesel engines and gas turbines. Tar can condense or polymerize to more complex structures in the pipes, filters or heat exchangers, causing process equipment problems (as choking and attrition), decreasing total efficiency, and increasing the cost of the process [3]. Because of the prohibition of direct gas stream utilisation, gas purification systems are needed.

Tar removal technologies including cracking and mechanical separation using scrubbers or cyclones take place downstream the gasifier (hot gas cleaning). Tar treatment inside the gasifier may eliminate the need for downstream cleanup. For both tar removal technologies, catalytic steam reforming is very promising [3] however it is a endothermic process and the external source of heat is needed [8]. This process usually involves tar components oxidation on supported nickel-based catalyst, with the use of steam, at the temperatures above 650 °C. Tar steam reforming leads to CO and H_2, enriching gas from biomass gasification in these components. The reaction pathway is described by reactions (1) and (2). Hydrocarbons react irreversibly to CO and H_2. A competing reaction leading to coke formation on the catalyst surface can be prevented by selecting the type of catalyst, steam to carbon ratio and reaction temperature [1].

$$C_xH_y + xH_2O = xCO + (x + y/2)H_2 \quad (1)$$

$$CO + H_2O = CO_2 + H_2 \quad (2)$$

Steam reforming catalysts for biomass tar decomposition should be efficient in reforming process,

A. Łamacz (✉) · A. Krztoń
Polish Academy of Sciences, Centre of Polymer and Carbon Materials, Marii Curie-Sklodowskiej 34, 41-819 Zabrze, Poland
e-mail: agata.lamacz@cmpw-pan.edu.pl

A. Musi · P. D. Costa
Laboratoire de Réactivité de Surface, Université Pierre et Marie Curie, CNRS UMR 7609, case 178, 4 place Jussieu, 75252 Paris, France

have high selectivity for syngas production, high resistance for carbon formation and attrition—in the case of fluidized bed application [2]. Carbonates like dolomite, or silicates like olivine are often used as inexpensive biomass tar decomposition catalysts [3, 9]. Nickel catalysts are the most often studied for their tar destruction ability and high activity in steam reforming.

Ceria-zirconia supported metallic phase (Ni, Pt, Pd) was found to be very promising catalysts system in reforming reactions. $Ni/CeZrO_2$ has been successfully applied to reforming and partial oxidation of methane. According to reactions 3–6, methane is adsorbed.

$$CH_4 + 2^* \rightarrow CH_{3^*} + H^* \quad (3)$$

$$CH_{3^*} + * \rightarrow CH_{2^*} + H^* \quad (4)$$

$$CH_{2^*} + * \rightarrow CH^* + H^* \quad (5)$$

$$CH^* + * \rightarrow C^* + H^* \quad (6)$$

$$C^* + O_o^x \rightarrow CO^* + V_o^{\bullet\bullet} + 2e' \quad (7)$$

$$V_o^{\bullet\bullet} + 2e' + O* \Leftrightarrow O_o^x + * \quad (8)$$

on active site of ceria-based materials (*), forming intermediate surface hydrocarbon species (CH_x*). Finally, carbon deposit (C^*) reacts with lattice oxygen (O_o^x) (reaction 7) continuously supplied by H_2O or CO_2 decomposition to O^* on reduced-state catalyst (reaction 8) [10, 11].

The addition of ZrO_2 to ceria improves oxygen storage capacity (OSC), redox properties, thermal stability, and catalytic activity [12–15]. High oxygen mobility and OSC makes ceria-zirconia very interesting in wide range of application involving catalytic reforming reactions. High temperature reaction between hydrocarbon and lattice oxygen can produce CO and H_2. The great benefit of $Ce_xZr_{1-x}O_2$ is its high resistance for carbon deposition [11]. The highest activity revealed $Ni/Ce_{0.7}Zr_{0.3}O_2$ catalysts. These catalysts also exhibit the highest resistance towards carbon deposition during steam reforming of methane [10, 16, 17].

Due to current requests in the field of energetic and the need of renewable energy sources application, we are focused on finding active catalyst for biomass tar decomposition. The goal of this work was to understand the chemistry involved in tar reforming process, using toluene as a model compound because it is one of major components of biomass tar (14 wt%), it is the most reactive among all tar components and it represents a stable aromatic structure in tar formed in high-temperature processes. In this study, ceria-zirconia supported Ni and Co catalysts were characterized and tested in toluene steam reforming reaction.

2 Experimental

2.1 Catalyst Preparation

Nickel and cobalt catalysts, each containing 1 and 10 wt% of active phase, were obtained by incipient impregnation of commercial ceria-zirconia CZ 70/30 (RHODIA Electronics & Catalysts) with different quantities of $Co(NO_3)_3 \cdot 6H_2O$ and $Ni(NO_3)_2 \cdot 2H_2O$ water solutions. Ceria-zirconia support was previously calcined at 500 °C for 5 h. Each mixture after impregnation was slowly dried in two steps: at room temperature overnight and at 110 °C. Finally, catalysts were calcined at 700 °C for 2 h. In this way 4 catalysts: Co(1)/CZ, Co(10)/CZ, Ni(1)/CZ, and Ni(10)/CZ were obtained.

2.2 Catalyst Characterization

Obtained catalysts were characterized by S_{BET}, X-ray diffraction (XRD), high resolution transmission electron microscopy (HRTEM), UV-Vis diffuse reflectance spectroscopy, temperature programmed reduction (TPR), and temperature programmed desorption (TPD). Specific surface areas were determined using Sorptomatic 1800 analyzer equipped in MILESTON100 software. XRD patterns were acquired using Siemens 500D diffractometer employing Cu-Kα radiation ($\lambda = 1{,}54$ Å). High resolution transmission electron microscopy (HRTM) was performed to determine the size of cobalt and nickel oxide particles on ceria-zirconia and to check their dispersion. HRTM studies were performed on a JEOL-JEM 2011 HR apparatus associated with a top entry device and operating at 200 kV. Diffuse reflectance spectra were recorded at room temperature between 200 and 900 nm on a Varian Cary 5E spectrometer equipped with a double monochromator and an integrating sphere coated with polytetrafluoroethylene (PTFE) which was used as a reference. H_2-TPR measurements were performed on a Autochem 2910 apparatus. All samples (50 mg) were treated by gas mixture of 5% H_2 in Ar and flow rate of 30 ml/min. The temperature was ramped linearly to 1,000 °C with heating rate of 7.5 °C/min. All TPR measurements were preceded by a temperature programmed oxidation (TPO) under 10% O_2 in He to 500 °C with the same temperature ramp as for TPR. TPD of toluene and catalytic tests were performed in U-type reactor. Gas in the outlet of reactor was analyzed by CO, CO_2 detectors and FID. For toluene-TPD execution, catalysts samples were treated by gas mixture consisting of toluene (1,000 ppm) and Ar as a balance at room temperature for 1 h. After toluene adsorption, samples were purged by Ar for 1 h. TPD was carried out in Ar with flow-rate of 250 mL/min and heating-rate of 3 °C/min from room temperature to 550 °C (Table 1).

Table 1 Specific surface area for CZ, Cu/CZ, and Co/CZ catalysts

Catalyst	S_{BET} [M^2/g]
CZ	136
Co(1)/CZ	106
Co(10)/CZ	98
Ni(1)/CZ	127
Ni(10)/CZ	100

2.3 Activity Measurements

Temperature programmed surface reactions (TPSR) were performed in quartz U-type reactor in the presence of 1,000 ppm toluene and 1.7% of steam in Ar as a balance. The flow-rate of 250 mL/min, heating-rate of 3 °C/min from 150 to 900 °C and GHSV = 30,000 h^{-1} were used during TPSR experiments. Catalytic tests in stationary conditions were performed in the presence of 2,000 ppm of toluene and 4% of steam in Ar as a balance with GHSV = 10,000 h^{-1}. The outlet gas composition during isotherms in temperatures decreasing from 900 to 400 °C was being detected by gas chromatograph until H_2, CO, and CO_2 concentrations were stable. Vapours were generated in saturators placed in ultra cryostat (toluene) and thermostat (steam). Toluene concentration was proved by CO_2 detection during its total oxidation in air on platinum catalysts at 850 °C. The scheme of the installation used for reforming tests in stationary conditions is shown on Fig. 1.

3 Results and Discussion

3.1 Catalysts Characterization

Specific surface areas of the support and catalysts are set-up in Table 2. It was observed, that with increasing metal loading surface area decreases.

3.2 X-ray Diffraction (XRD)

XRD patterns of the support and catalysts are shown on Figs. 2 and 3.

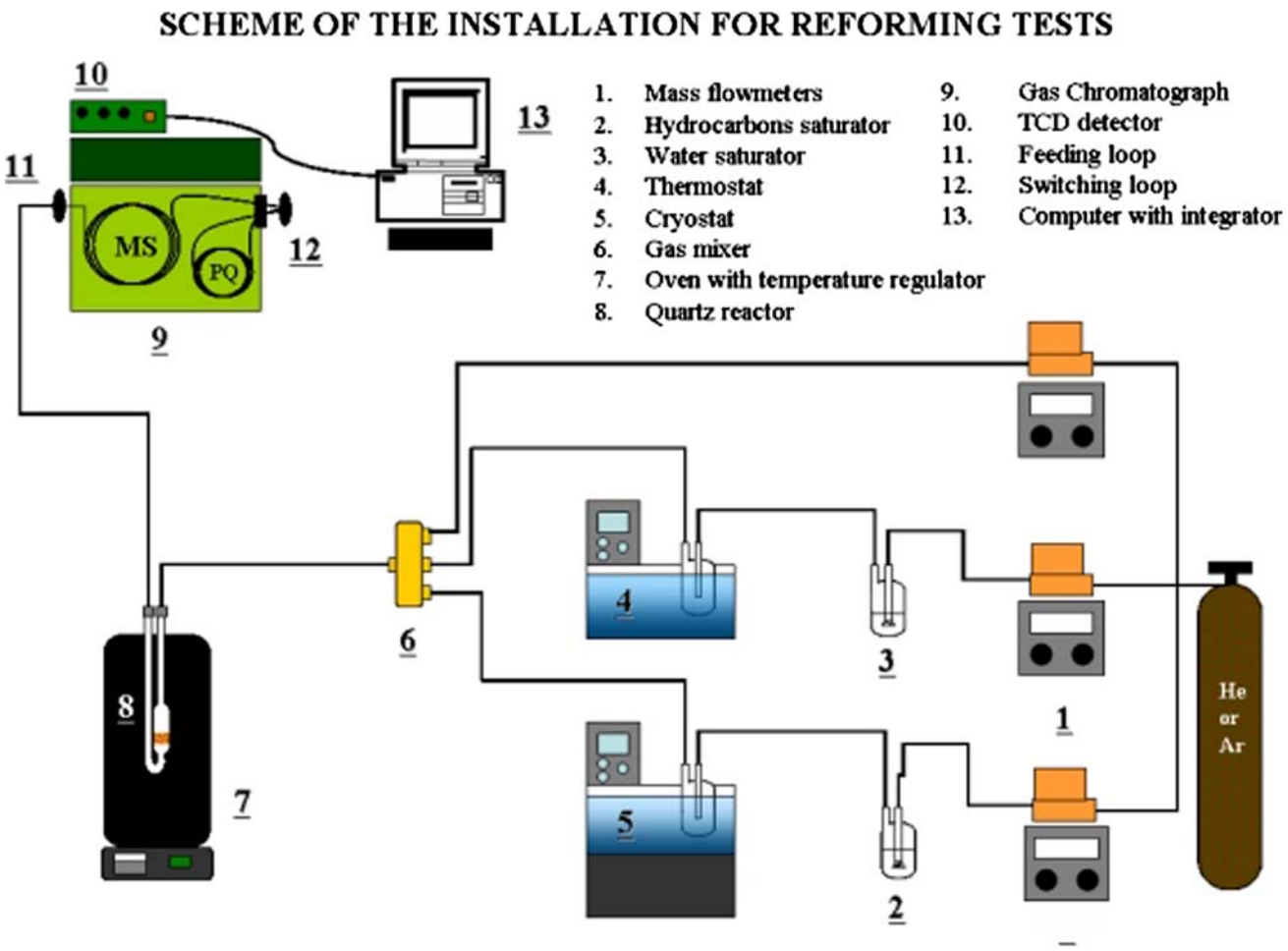

Fig. 1 Scheme of the installation for reforming tests

Table 2 H_2/CO ratios for Ni/CZ and Co/CZ catalysts at stationary conditions

	H_2/CO at different T						
	900 °C	800 °C	700 °C	600 °C	500 °C	450 °C	400 °C
Ni(1)/CZ	–	2.6	2.4	2.5	4.5	6.2	12.2
Ni(10)/CZ	2.8	2.5	2.7	3.2	4.1	7.9	16.7
Co(1)/CZ	3.0	3.8	7.1	20.2	–	–	–
Co(10)/CZ	2.5	2.4	2.8	3.1	5.3	–	1.1

Co_3O_4 crystallites did not appear for low loaded catalyst (Fig. 2a). XRD pattern of Co(10)/CZ clearly shows Co_3O_4 crystallites presence. High Co loading takes effect in cobalt oxide particles agglomeration which is probably caused by metal–metal interaction (Fig. 2c).

The same refers to Ni/CZ catalysts (Fig. 3). Low loading of Ni did not influence the support lattice. No changes on CZ XRD pattern after impregnation were seen. Sharp NiO peaks indicate its bad dispersion on ceria-zirconia (Fig. 3c). Due to favoured metal–metal interaction, the formation of NiO crystallites was observed in case of Ni(10)/CZ [18, 19].

3.3 TEM Observations

Support TEM image is presented on Fig. 4. Visible, big crystallites (6–10 nm) are caused by support's sintering. Material's structure is irregular and partially amorphous [20].

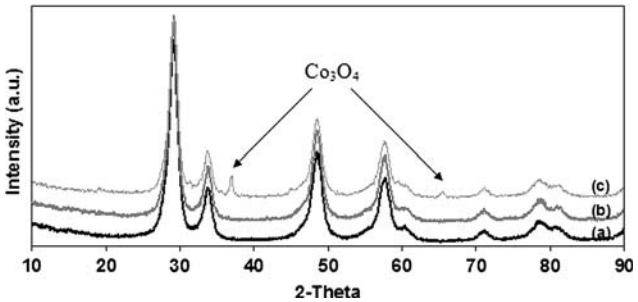

Fig. 2 XRD spectra for CZ (**a**), Co(1)/CZ (**b**), and Co(10)/CZ (**c**)

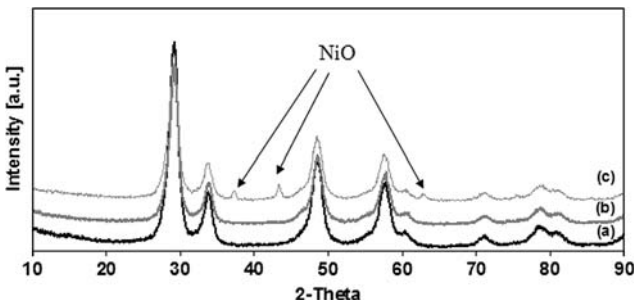

Fig. 3 XRD spectra for CZ (**a**), Ni(1)/CZ (**b**), and Ni(10)/CZ (**c**)

High loaded Co catalyst is heterogeneous and metallic phase is not dispersed well on the support's surface. Co_3O_4 crystallites of diameters from 50 to 80 nm are shown on Fig. 5. On area signed as "A" Co_3O_4 agglomeration is shown (87 × 62 nm^2). "B" area shows support's particles and isolated Co_3O_4 crystals. Approximation of area "C" presents Co_3O_4 crystallite of 50 nm diameter.

TEM analysis of Ni(10)/CZ (Fig. 6) revealed its homogeneity. Global and local analysis for this catalyst, like in case of Cu(10)/CZ are similar.

3.4 UV-Vis Diffuse Reflectance Spectroscopy

UV-VIS experiments performed for the support and catalysts revealed that their main adsorption peak occurs at 280 nm (Figs. 7 and 8). For low loaded catalysts the increase of absorption at this wavelength was observed according to ceria-zirconia. On high loaded catalysts, the decrease of spectral absorption was observed. In case of Co catalysts, an additional band (at 750 nm) occurs. With

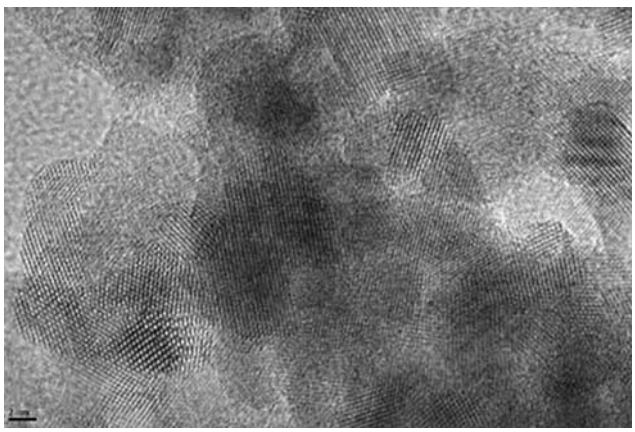

Fig. 4 TEM micrograph of the support (×600,000)

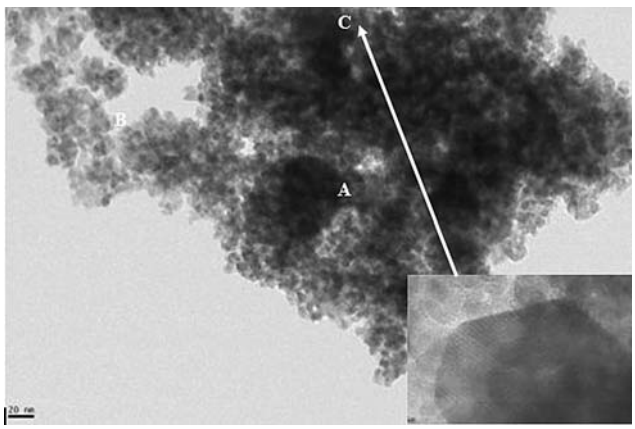

Fig. 5 TEM micrograph of Co(10)/CZ (×50,000)

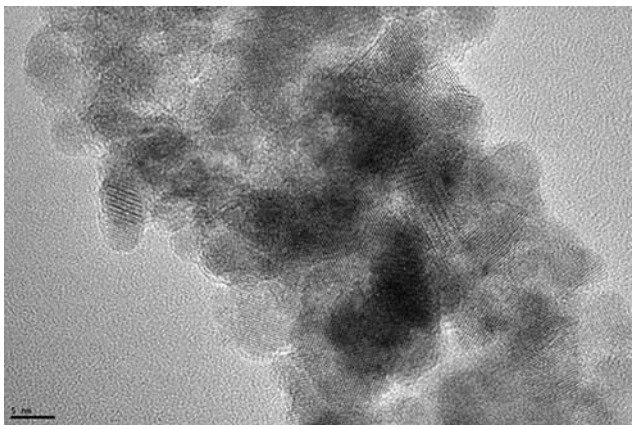

Fig. 6 TEM micrograph of Ni(1)/CZ (×400,000)

increasing metal phase content, the absorption in the range of 400–900 nm increases.

3.5 Temperature Programmed Reduction (TPR)

TPR-H_2 profiles for the support and Co/CZ catalysts are illustrated on Fig. 9.

The reduction peak at 550 °C is assigned to bulk CeO_2 reduction ($Ce^{4+} \rightarrow Ce^{3+}$) (Fig. 9a). Shoulder at 350 °C probably refers to CeO_2 surface reduction. The reduction peak at 350 °C on Fig. 9b corresponds to CoO reduction. The shoulder at 240 °C is probably due to reduction of Co_3O_4 to CoO. The first peak at 300 °C on Co(10)/CZ plot (Fig. 9c) is assigned to reduction of small amount of Co_3O_4. The second one, at 400 °C probably corresponds to CoO–Co reduction [21].

In case of Ni catalysts, two kinds of reduction peaks were observed. Peaks at 250 °C (for Ni(1)/CZ) and at 275 °C (for Ni(10)/CZ) are assigned to relatively free NiO reduction (Fig. 10). Peaks at 350 °C for both Ni/CZ are contributed to complex NiO, strongly interacting with the support [22].

3.6 Temperature Programmed Desorption (TPD)

Comparison of catalysts behaviour during TPD in the presence and in the absence of water is shown on Figs. 11–14. It was calculated, that in case of Co(1)/CZ, catalyst adsorbs more toluene in the presence of water. Toluene desorption occurs at low temperatures when there is no water in the inletting gas mixture (Fig. 11a). The absence of hydrocarbon desorption in the presence of water may be due to its blocking on catalyst's surface by water particles. Therefore, CO_2 formation above 300 °C is assigned to strongly adsorbed toluene oxidation.

For high loaded Co catalyst (Fig. 12a), toluene adsorbed in the absence of water desorbs at low temperatures. Its oxidation is bimodal and it starts at 80 °C. Low-temperature CO_2 production is attributed to slightly bounded toluene oxidation. High-temperature toluene oxidation is due to its strong adsorption on catalyst's surface. Shifting

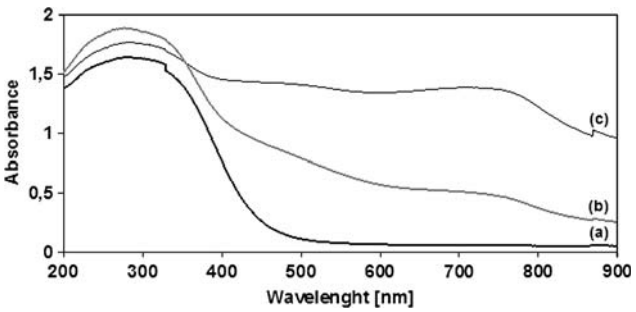

Fig. 7 UV Vis spectra of CZ (**a**), Co(1)/CZ (**b**), and Co(10)/CZ (**c**)

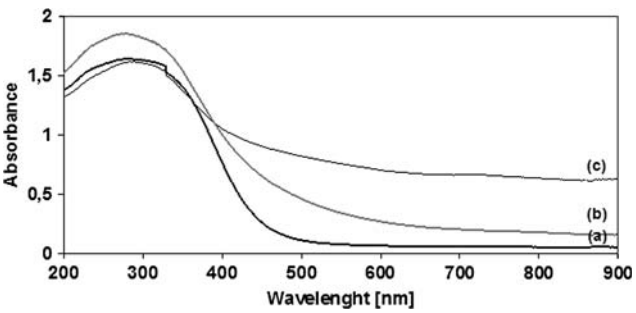

Fig. 8 UV Vis spectra of CZ (**a**), Ni(1)/CZ (**b**), and Ni(10)/CZ (**c**)

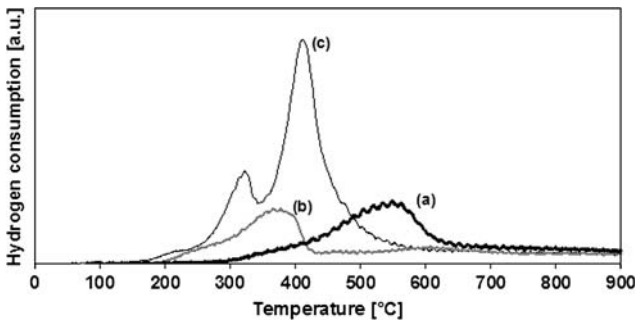

Fig. 9 TPR profiles of CZ (**a**), Co(1)/CZ (**b**), and Co(10)/CZ (**c**)

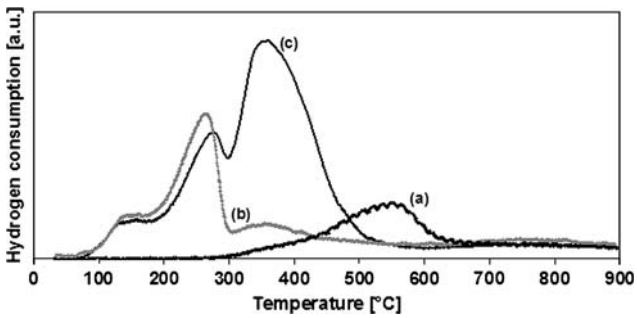

Fig. 10 TPR profiles of CZ (**a**), Ni(1)/CZ (**b**), and Ni(10)/CZ

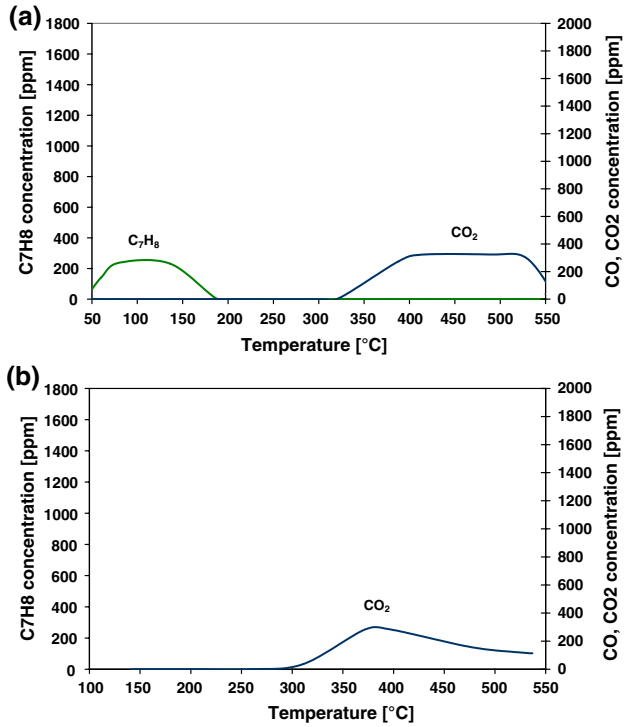

Fig. 11 TPD profiles of Co(1)/CZ in the absence (**a**) and in the presence (**b**) of water

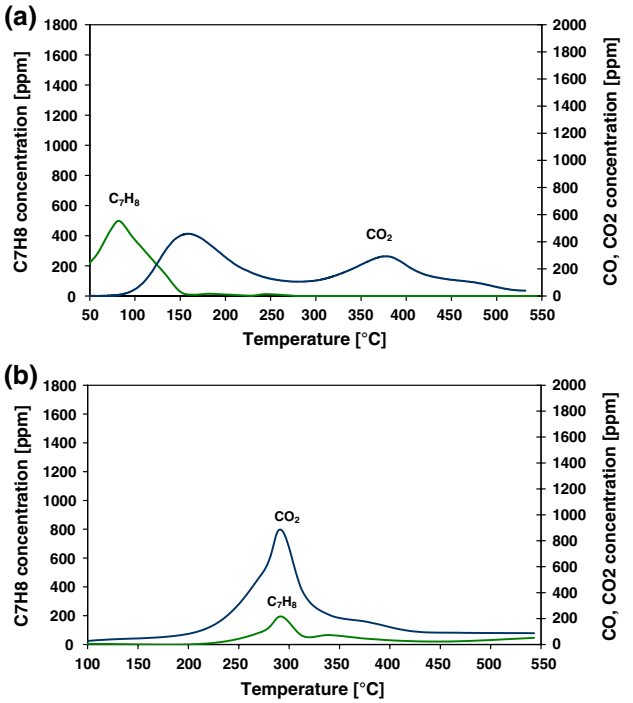

Fig. 12 TPD profiles of Co(10)/CZ in the absence (**a**) and in the presence (**b**) of water

of toluene desorption toward higher temperatures in case of TPD performed in the presence of water (Fig. 12b) may be explained by hydrocarbon blocking.

In case of low loaded Ni catalyst, it was observed that toluene desorption occurs only when water is present in the inlet gas (Fig. 13b). Hydrocarbon oxidation is bimodal and it proceeds at lower temperatures when comparing to non-water experiment.

It was noticed that during TPD for Ni(10)/CZ, CO_2 production occurs in the same temperature range for both kinds of experiments, although it is more significant when water is present (Fig. 14).

3.7 Catalytic Tests

3.7.1 Temperature Programmed Surface Reaction (TPSR)

Ceria-zirconia's TPSR profile (Fig. 15) reveals toluene's consumption up to 450 °C and bimodal toluene's oxidation. The CO_2 formation with maximum at 500 °C corresponds to slight toluene's oxidation. Reforming reaction starts at about 650 °C.

Figure 16 shows Co(1)/CZ TPSR. There's toluene consumption observed up to 550 °C. From 310 to 450 °C part of the toluene is oxidized to CO_2, whereas from 550 °C it starts to be completely converted to CO and CO_2. While CO concentration increases, toluene conversion to CO_2 begins decrease from 680 °C.

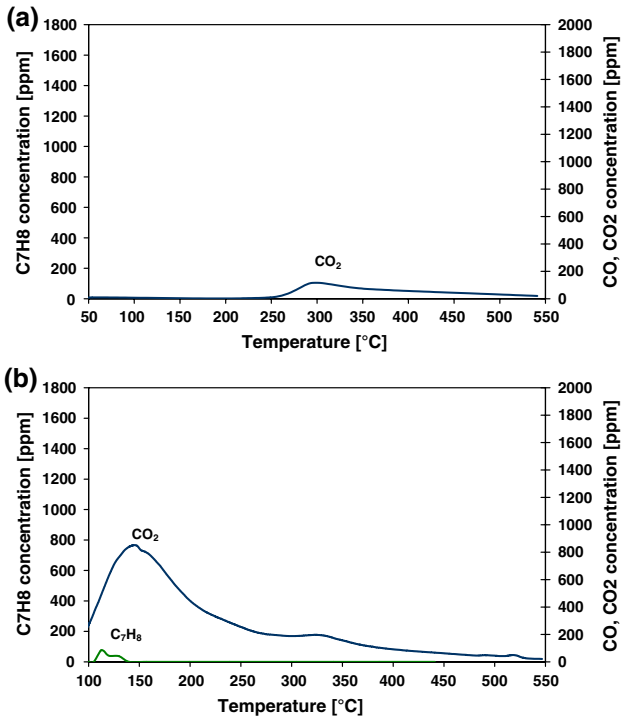

Fig. 13 TPD profiles of Ni(1)/CZ in the absence (**a**) and in the presence (**b**) of water

Analogically to low Co loaded catalyst, for Co(10)/CZ constant toluene consumption to 550 °C was observed. While CO concentration increases, CO_2 starts to decrease

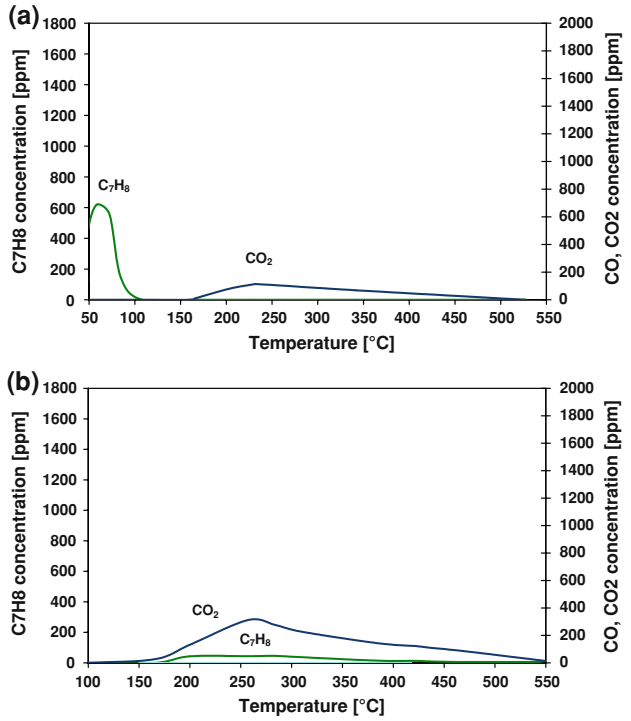

Fig. 14 TPD profiles of Ni(10)/CZ in the absence (**a**) and in the presence (**b**) of water

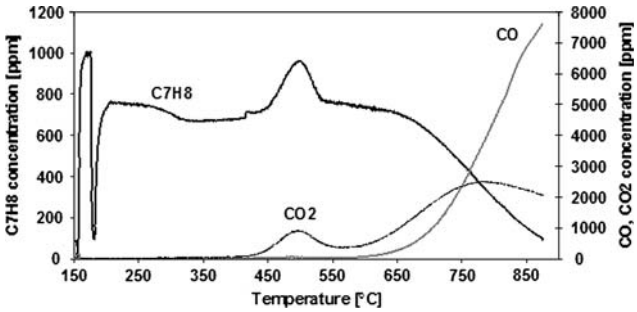

Fig. 15 TPSR of CZ

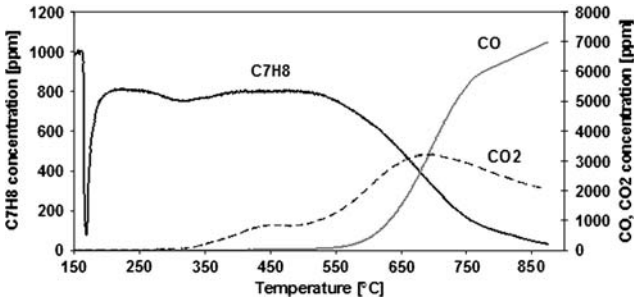

Fig. 16 TPSR of Co(1)/CZ

from 750 °C (Fig. 17). Higher toluene to CO conversion on Co(1)/CZ and more important CO_2 participation on Co(10)/CZ were noticed.

In case of Ni catalysts (Fig. 18 and 19) conversion of toluene to CO_2 up to 500 and 450 °C (for low and high loaded catalysts respectively) was also observed, nevertheless its complete oxidation started at 475 °C. It was noticed, that CO concentration was increasing while CO_2 was decreasing rapidly. Analogically to Co catalysts, more CO was produced on low loaded Ni/CZ.

Generally, toluene's oxidation to CO_2 may occur by the oxygen stored on catalyst's surface or by the oxygen produced in water decomposition reaction, taking place on ceria-zirconia surface (reaction 3). CO may be produced in steam reforming reaction (reaction 10) or by partial toluene oxidation (reaction 11).

$$H_2O \rightarrow H_2 + {}^1/_2O_2 \quad (9)$$

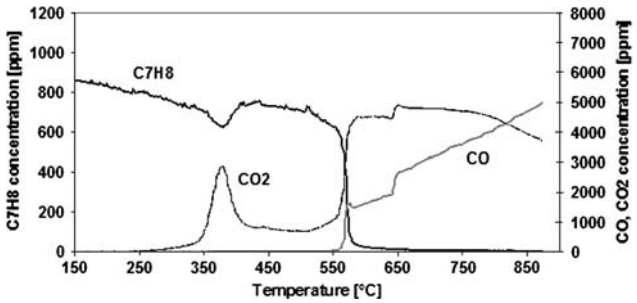

Fig. 17 TPSR of Co(10)/CZ

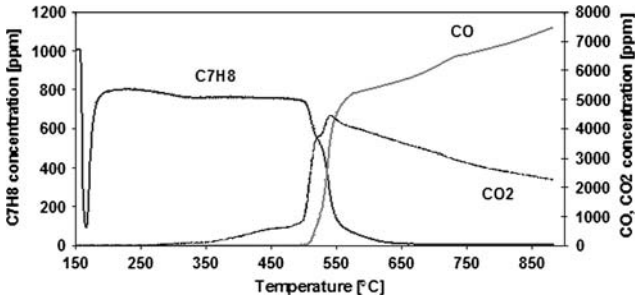

Fig. 18 TPSR of Ni(1)/CZ

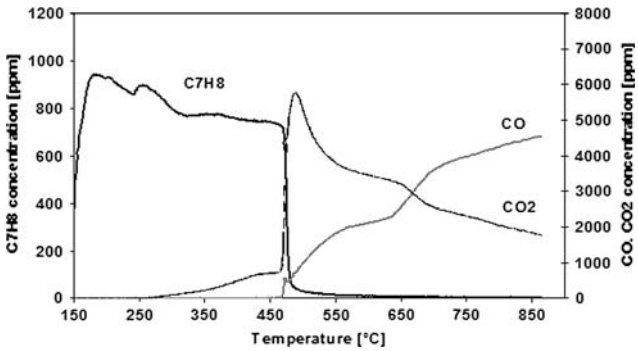

Fig. 19 TPSR of Ni(10)/CZ

$$C_7H_8 + 7H_2O \rightarrow 7CO + 11H_2 \quad (10)$$

$$C_7H_8 + 3^1/_2\ O_2 \rightarrow 7CO + 4H_2 \quad (11)$$

3.7.2 Catalytic Tests in Stationary Conditions

The effect of metal loading and temperature on toluene conversion and product yields for Co/CZ and Ni/CZ catalysts are shown on Figs. 20–22. Toluene conversion increased with temperature as it was expected. It was observed that with the increase of nickel loading conversion of toluene decreased, while the increase of cobalt loading improved hydrocarbon conversion (Fig. 20). At 700 °C all catalysts except Co(1)/CZ revealed 100% toluene conversion to CO and CO_2. For Ni(1)/CZ, CO yield achieved 100% at this temperature (Fig. 21). H_2 yield is constant at high temperatures and it starts do decrease with temperature decrease from 600 ° (Fig. 22). Both Ni/CZ catalysts and high loaded Co/CZ revealed similar behavior in isothermal conditions. Co(1)/CZ has revealed poor conversion and CO and H_2 yields even at 700 °C.

Table 2 shows H_2/CO ratios for all tested catalysts. A number of H_2 moles per one produced mol of CO for Ni(1)/CZ, Ni(10)/CZ, and Co(10)/CZ at temperature range from 900 to 700 °C were almost equal and almost 2.9. It means that at high temperatures, except steam reforming, reverse water gas shift (reaction 12) and dry reforming (reaction 13) occur as side reactions.

$$C_7H_8 + 7H_2O = 7CO + 11H_2 \quad (10)$$

$$CO_2H_2 \Leftrightarrow CO + H_2O \quad (12)$$

$$C_7H_8 + 7CO_2 = 14CO + 4H_2 \quad (13)$$

With the decrease of temperature, toluene conversion decreased and H_2/CO ratio increased, implying that WGS reaction was becoming more and more predominant.

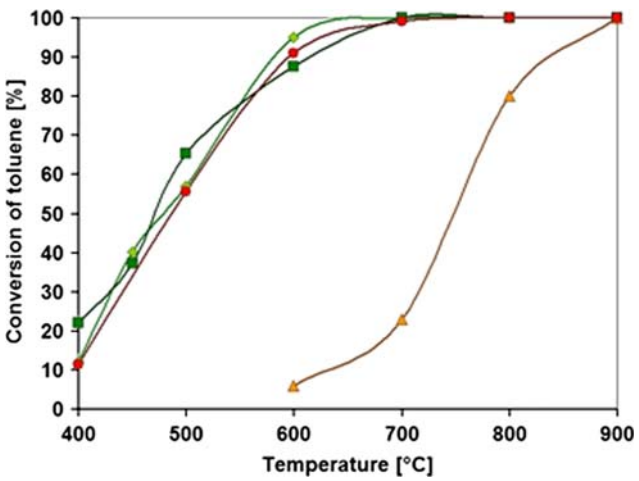

Fig. 20 Toluene conversion for Ni(1)/CZ (◇), Ni(10)/CZ (■), Co(1)/CZ (▲), and Co(10)/CZ (●)

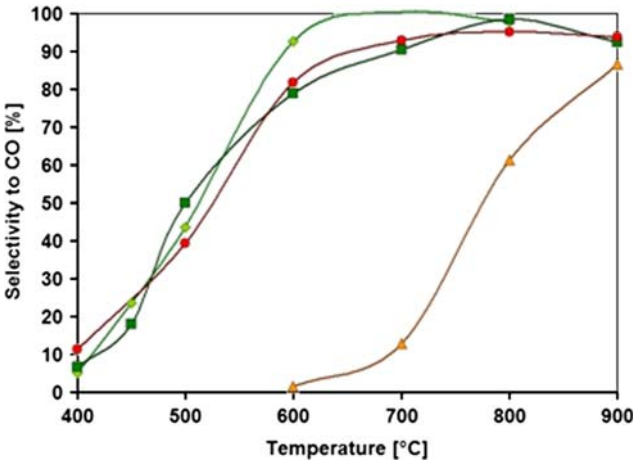

Fig. 21 CO yield for Ni(1)/CZ (◇), Ni(10)/CZ (■), Co(1)/CZ (▲), and Co(10)/CZ (●)

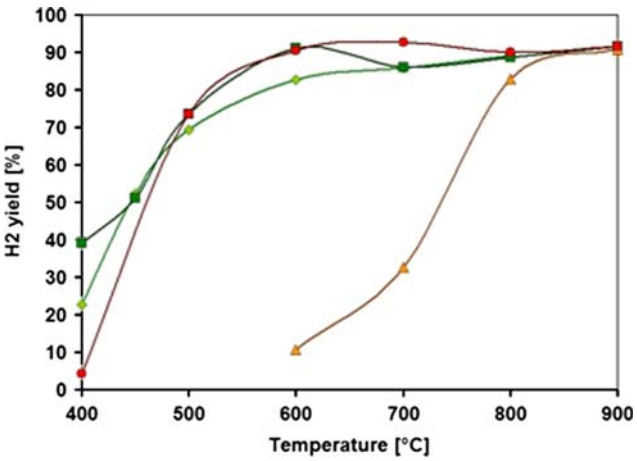

Fig. 22 H_2 yield for Ni(1)/CZ (◇), Ni(10)/CZ (■), Co(1)/CZ (▲), and Co(10)/CZ (●)

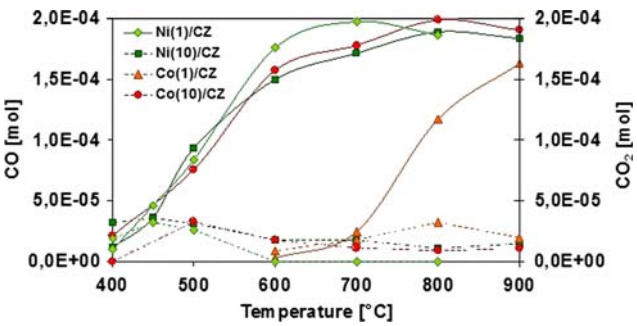

Fig. 23 CO (—) and CO_2 (- - -) production on Ni(1)/CZ (◇), Ni(10)/CZ (■), Co(1)/CZ (▲), and Co(10)/CZ (●)

Figure 23 shows quantities of CO and CO_2 during catalytic test in stationary conditions. It was observed, that with the decrease of temperature, CO_2 production enlarges, but it exceeds CO production not before 400 °C. From

900 °C until 500 °C CO production is still predominant for both Ni/CZ and for high loaded Co/CZ.

Durability tests will be performed in the near future.

4 Conclusions

XRD analysis indicated the presence of Co_3O_4 and NiO crystallites only for high loaded catalysts. TEM observations for Co(10)/CZ revealed that Co was not well dispersed, forming clusters, the catalyst is heterogeneous. In the case of Ni(10)/CZ, metallic phase was well dispersed and the catalysts was texturally homogeneous. TPR experiments showed the reduction of Co_3O_4 and CoO for both low and high loaded catalysts. In the case of Ni/CZ, some free NiO reduction was observed, and the reduction of NiO in strong interaction with ceria-zirconia was detected. During TPD experiments, toluene was found to desorb at low temperature. Bimodal toluene oxidation occurred for Co(10)/CZ. Simultaneous toluene desorption with CO_2 formation on all samples indicates two kinds of hydrocarbon adsorption on the catalyst surface—weak and strong. Toluene desorption and CO_2 production were shifted towards higher temperatures for experiments performed in the presence of H_2O, what can be explained by the inhibition of active sites by water. TPSR experiments revealed good results towards CO production, which was more significant on low loaded catalysts. Nevertheless, total oxidation of toluene occurred at lower temperatures for high loaded catalysts. In the case of Co/CZ, two regions of toluene oxidation were observed, while on Ni/CZ CO production occurred at lower temperatures. WGS reaction took place below 700 °C and its participation was increasing with decreasing T. All catalysts presented a very good stability at the temperature range between 400 and 900 °C. Ceria-zirconia based catalysts utilize unreduced state and they should demonstrate good activity in oxidizing conditions in reforming reaction. Ni/CZ catalysts were active in toluene steam reforming reaction from 400 °C (40% of toluene conversion) and seemed to be very promising in biomass tar decomposition. TG analysis in air, performed after 34 h of catalytic test in stationary conditions have shown that total weight loss for Ni(1)/CZ during temperature increase from 150 to 860 °C amounted 1 wt%. It indicates that ceria-zirconia supported catalysts were resistant to carbon deposition.

Acknowledgment Authors acknowledge financial support of the Ministry of Science and Higher Education (project No PBZ-MEN-2/2/2006) and International Group of Research (GDRI) "Catalysis for Environment: Depollution, Renewable Energy and Clean Fuels". We are also very grateful to Prof. Gerald Djega-Mariadassou for fruitful discussion and to Ms. Sylwia Czajkowska for an additional chromatographic and TG analysis.

References

1. Coll R, Salvado J, Farrioli X, Montane D (2001) Fuel Process Technol 74:19–31
2. Swierczynski D, Courson C, Kiennemann A (2008) Chem Eng Process 47:508–513
3. Swierczynski D, Libs S, Courson C, Kiennemann A (2007) Appl Catal B 74:211–222
4. Bridgwater AV (1995) Fuel 74:631–653
5. Mojtahedi W, Bacman R (1989) J Inst Energy 62:189–196
6. Narvaez I, Corella J, Orio A (1997) Ind Eng Chem Res 36:317–327
7. Kinoshita CM, Wang Y, Zhou JC (1994) J Anal Appl Pyrolysis 29:169–181
8. Cheekatamarla PK, Finnerty CM (2006) J Power Sources 160:490–499
9. Devi L et al (2007) Fuel Process Technol 86:707
10. Laosiripojana N, Assabumrungrat S (2005) Appl Catal B 290:200–211
11. Laosiripojana N, Assabumrungrat S Appl Catal B (in press)
12. Balducci G, Kaspar J, Fornasiero P, Graziani M, Islam MS (1998) J Phys Chem B 102:557
13. Roh HS, Dong WS , Jun KW, Park SE (2001) Chem Lett 88
14. Fornasiero P, Dimonte R, Rao GR, Kaspar J, Meriani S, Trovarelli A, Graziani M (1995) J Catal Lett 151:168
15. Rao GR, Kaspar J, Meriani S, Dimonte R, Graziani M (1994) J Catal Lett 24:107
16. Ramirez-Cabrera E, Atkinson A, Chadwick D (2004) Appl Catal B 47:127
17. Ramirez-Cabrera E, Laosiripojana N, Atkinson A, Chadwick D (2003) Catal Today 78:433
18. Amin NAS et al (2003) Appl Catal B 43:57–69
19. Biswas P, Kunzru D (2007) J Hydrogen Energy 32:969–980
20. Stark WJ et al (2005) J Catal 220:35–43
21. Saib AM et al (2006) J Catal 239:326–339
22. Roh HS, Jun KW, Dong WS, Chang JS, Park SE, Joe YI (2002) J Mol Catal A: Chem 181:137–142